Low-rank modeling of primary atomization

By D. J. Bodony†, P. Sashittal† AND A. Towne‡

A three-step, data-driven method is presented for developing low-rank models of primary atomization from sharp interface volume-of-fluid data. In the first step, the interface-normal velocity is estimated using the Horn-Schunck method, an optical flow technique. In the second step, data reduction is performed on the interface-normal velocity using dynamic mode decomposition. In the third and final step, the reduced interface-normal velocity is used to advect the volume-of-fluid field forward in time. The method is evaluated on simulation data from the primary atomization of a planar liquid jet.

1. Introduction

Liquid sprays play a key role in many environmental flows and engineering devices. Fuel sprays for combustion systems represent arguably the most impactful class of engineering sprays in our society. Multiphase flow research is entering an exciting era where the development of algorithms, models, and experimental diagnostics are enabling physics-driven studies of spray control. Recent advances in liquid-gas flow algorithms make simulations of turbulent spray breakup and dispersion under realistic conditions possible. Simultaneously, improvements in the national research computing resources permit massive calculations that revolutionize our understanding of multiphase flows while recent progress in experimental diagnostics for liquid-gas flows provides validation data of unprecedented quality. Capitalizing on these advancements is essential to developing the critical science infrastructure needed to meaningfully impact fuel sprays, and thus to improve the efficiency, robustness, and environmental impact of hydrocarbon combustion.

Towards the goal of achieving multiphase flow control, this work is motivated by the lack of adequate reduced-order models (ROMS) for predicting primary atomization. Experience-guided control is commonly used in microfluidic systems, subsurface oil reservoirs, electrostatic and ultrasonic atomizers, and spray nozzle design (Shui *et al.* 2007; Jansen *et al.* 2008; Marsh *et al.* 1988; Kushari *et al.* 2001; Hunter 1969; Neumeier & Zinn 1996). Algorithm-based control is limited and focused on fluid systems for which reduced-order models are available, like oil-water separation in porous subsurface oil reservoirs and thermo-acoustic instabilities (Jansen *et al.* 2008; Dowling & Morgans 2005). We seek to enable physics-guided reduced order model-based control of primary atomization by developing model reduction techniques for volume-of-fluid-like data, such as from experimental imaging techniques (e.g., X-ray and shadowgraphy), suitable for use in hardware-in-the-loop control.

This report proceeds by describing the simulation that generated the test data in Section 2, followed by the image processing techniques used to construct the interface-normal velocity field in Section 3. Section 4 presents the reduced order velocity field using dynamic mode decomposition. In Section 5 the data reconstruction is applied and compared to the original data. The report concludes with a summary in Section 6.

† Department of Aerospace Engineering, University of Illinois at Urbana-Champaign
‡ Center for Turbulence Research, Stanford University

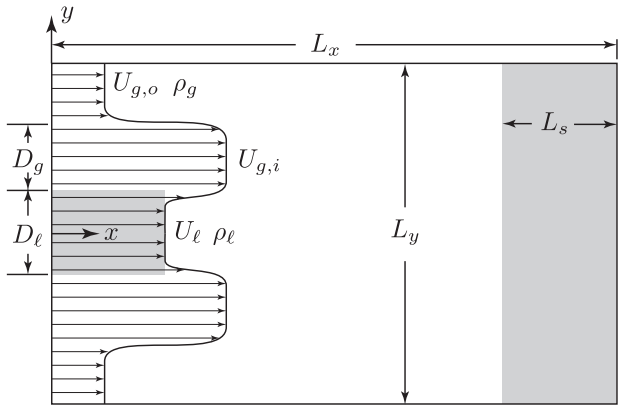

FIGURE 1. Planar liquid jet atomization domain with relevant scales. Left-most grey region indicates liquid column width while right-most grey region indicates sponge region.

Parameter	Value	Parameter	Value
D_g	5	ρ_g	1.2×10^{-3}
L_x	10	$v_{\max}$	0.25
L_y	10	σ	0.5
L_s	1.5	ω	$\pi/4$, $\pi/2$, $3\pi/4$, π
$U_{g,i}$	10	ϕ	π
$U_{g,o}$	10		

TABLE 1. Simulation parameters defined in Figure 1 and Eq. (2.1).

2. Database: primary atomization of a planar liquid jet

A planar liquid jet with gas co-flow is studied in the configuration shown in Figure 1. The low-cost, two-dimensional problem was used in favor of a three-dimensional simulation representing a specific experiment. The imposed velocity profile shown in figure 1 used hyperbolic tangent functions. The liquid-gas interface at $y = \pm D_\ell/2$ was perturbed by an imposed vertical velocity of the form

$$v(0, y, t) = v_{\max} \left\{ e^{-(y-1/2)^2/\sigma^2} \sin(\omega t) + e^{-(y+1/2)^2/\sigma^2} \sin(\omega t + \phi) \right\}. \qquad (2.1)$$

The parameters used are given in Table 1 where all quantities are normalized by the liquid jet diameter, D_ℓ, the liquid jet velocity, U_ℓ, and the liquid jet density, ρ_ℓ. In addition, the Weber number was $\mathrm{We} = \rho_g U_g^2 \delta_g/\gamma = 33$, where δ_g is the inflow vorticity thickness and γ is the surface tension. The liquid- and gas-phase Reynolds numbers were $\mathrm{Re}_\ell = \rho_\ell U_\ell D_\ell/\mu_\ell = 1 \times 10^6$ and $\mathrm{Re}_g = \rho_g U_g D_g/\mu_g = 3.5 \times 10^6$.

The simulations were carried out using the NGA multiphase solver (Desjardins *et al.* 2008). The initial condition was a quiescent gas with the inflow liquid and gas velocity fields imposed for $t > 0$. The upper and lower boundaries ($y = \pm L_y/2$) were slip walls and the $x = L_x$ boundary was an outflow. A sponge region was included in $L_x - L_s \le x \le L_x$. A uniformly-spaced grid of size of $(N_x, N_y) = (500, 500)$ was used.

The simulations, one for each value of ω listed in Table 1, were carried out from the initial condition until a time of approximately $t = 50 D_\ell/U_\ell$. Simulation volume-of-fluid (VOF) data were saved at an interval of $10^{-2} D_\ell/U_\ell$. Three sample snapshots of the

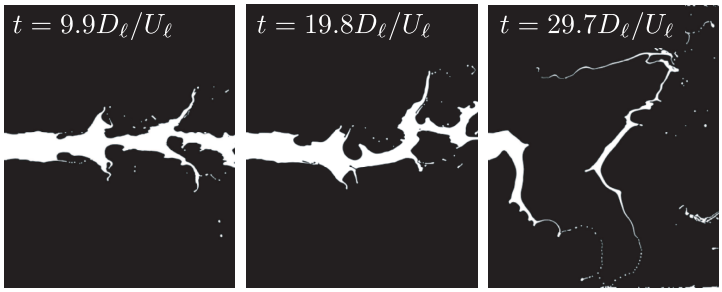

FIGURE 2. Volume-of-fluid snapshots at the indicated times for $\omega = \pi$ forcing simulation. Fluid is in white while gas is in black.

VOF field, $\mathcal{V}(\vec{x}, t)$, are shown in Figure 2 for the forcing frequency of $\omega = \pi$. (The sponge zone region has been omitted.) The simulation-generated $\mathcal{V}(\vec{x}, t)$ databases are used in subsequent analyses. Only data from the simulation with $\omega = \pi$ are presented in this report.

3. Image processing of volume-of-fluid data

The VOF field represents the fractional volume the liquid occupies in a computational cell and takes the values of 1 and 0 for liquid-only or gas-only conditions, respectively. Cells that are partially filled with liquid acquire an intermediate value. The VOF is computed as the cell average of the liquid volume fraction, f, which is transported by the (assumed incompressible) carrier fluids as

$$\frac{\partial f}{\partial t} + \frac{\partial u_i f}{\partial x_i} = 0, \tag{3.1}$$

where u_i is the ith component of the fluid (liquid or gas) velocity. Because it is assumed that $\vec{u}$ is not known, a PDE-based update like Eq. (3.1) is not available for either f or $\mathcal{V}$ for model reduction.

Instead, the future evolution of $\mathcal{V}$ will be inferred from past data, as follows. It is supposed that a collection $\mathsf{W}_0^N = [\mathcal{V}(\vec{x}, t_0)\, \mathcal{V}(\vec{x}, t_1) \ldots \mathcal{V}(\vec{x}, t_N)]$ of data are available for times $t_0 < t_1 < \cdots < t_N$ which are assumed to be separated by a constant timestep Δt. Because W_0^N represents the time evolution of a (nearly) spatially discontinuous field, applying standard model reduction techniques, such as those based on projection (proper orthogonal decomposition (POD) (Holmes *et al.* 1996) or dynamic mode decomposition (DMD) (Schmid 2010)), to $\mathcal{V}$ directly to it will introduce spurious spatial artifacts because of the spatial discontinuities in the data.

Because the VOF data are continuous in time, it is supposed that there exists an underlying velocity-like field $\vec{v}$ that advects $\mathcal{V}$ according to the simple optical flow map

$$\mathcal{V}(\vec{x}, t + \mathrm{d}t) = \mathcal{V}(\vec{x} - \mathrm{d}\vec{x}, t) \tag{3.2}$$

where the displacement vector $\mathrm{d}\vec{x}$ is given by

$$\mathrm{d}\vec{x} = \int_t^{t+\mathrm{d}t} \vec{v}\, \mathrm{d}t. \tag{3.3}$$

Equation (3.2) precludes any topology changes in $\mathcal{V}$ but enables the use of image processing techniques to estimate $\vec{v}$ in the direction normal to the liquid-gas interface.

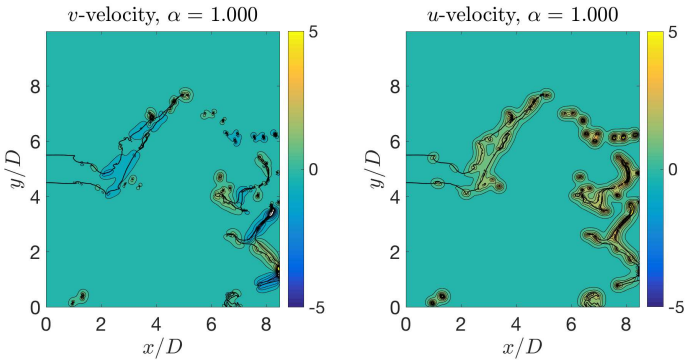

FIGURE 3. Sample interface-normal velocity field estimated with the (Horn & Schunck 1981) algorithm. Velocity is in units of U_ℓ.

The global estimation method of Horn & Schunck (1981) defines the interface-normal velocity $\vec{v}$ as the vector field that achieves the minimum

$$\vec{v} = \arg\min_{\vec{V}} \int (\mathcal{V}_t + \vec{V}\cdot\nabla\mathcal{V})^2 + \alpha||\nabla\mathcal{V}||_2^2 \,\mathrm{d}A \tag{3.4}$$

where the first quadratic term enforces Eq. (3.2), the second term enforces smoothness of the resulting vector field $\vec{v}$, and the integration is over the entire image. The operator ∇ computes the gradient, or edge, of $\mathcal{V}$; the Sobel edge detection algorithm (Pratt 2006) is used for ∇. The parameter α controls the smoothness of the resulting vector field, with larger α values indicating smoother fields. An example interface-normal vector field is shown in Figure 3 for $\alpha = 1$.

4. Model reduction

Because the vector field $\vec{v}$ is smooth in space and time, standard model reduction techniques can be applied to it. The DMD method of Schmid (2010) is chosen because of its demonstrated use in low-rank dynamical systems. Using the interface normal velocity $\vec{v}$, the data matrix $\mathsf{V}_0^N = [\vec{v}(\vec{x},t_0)\,\vec{v}(\vec{x},t_1)\,\ldots\,\vec{v}(\vec{x},t_N)]$ is formed such that a low-rank evolution operator A is constructed to minimize the error $||\mathsf{V}_1^N - \mathsf{A}\mathsf{V}_0^{N-1}||_F^2$. The operator $\mathsf{A}_{\mathrm{svd}}$ that achieves the minimum has rank m that is no greater than the rank of V_0^{N-1}. The rank can be further reduced to $r < m$ by taking the r-largest singular vectors, such that

$$\mathsf{A}_{\mathrm{DMD}}^r = \mathsf{U}_r^H \mathsf{V}_1^N \mathsf{V}_r \Sigma_r^{-1}, \tag{4.1}$$

where $\mathrm{svd}(\mathsf{V}_0^{N-1}) = \mathsf{U}_r\Sigma_r\mathsf{V}_r^H$ is the rank-r economy singular value decomposition of the unshifted data matrix V_0^{N-1}. Note that $\mathsf{A}_{\mathrm{DMD}}^r$ is an $r\times r$ operator of rank r.

Using Eq. (4.1) a low-rank approximation to $\vec{v}$, say $\vec{w}^r$, is constructed through the following sequence. The $N+1$ time snapshots of $\mathcal{V}$ data, W_0^N, are used to construct the N interface-normal velocity fields $\mathsf{V}_0^{N-1} = [\vec{v}(\vec{x},t_{1/2})\,\vec{v}(\vec{x},t_{3/2})\,\ldots\,\vec{v}(\vec{x},t_{N+1/2})]$. Note that intermediate times $t_{i+1/2}$ are used. The DMD procedure is then applied to V_0^{N-1} to construct $\mathsf{A}_{\mathrm{svd}}$ and r is chosen to get $\mathsf{A}_{\mathrm{DMD}}^r$. The low-rank interface-normal velocity

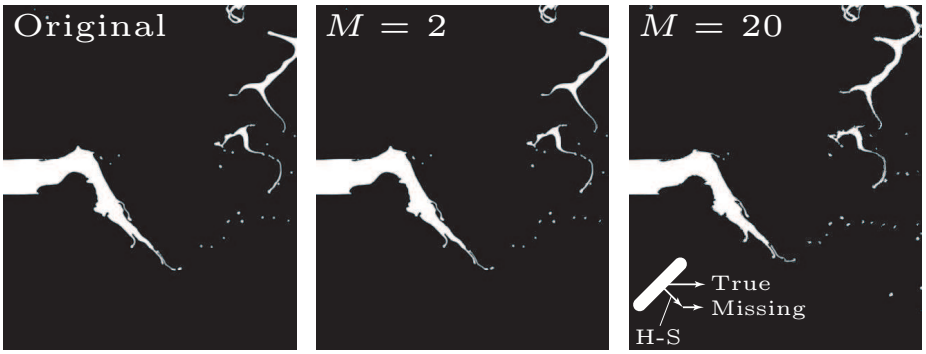

FIGURE 4. Demonstration of $\mathcal{V}$ reconstruction using rank $r = 9$ and two values of M.

field $\vec{w}_i^r$ can then be approximated using

$$\vec{w}_0^r \leftarrow \mathsf{U}_r^* \vec{v}_0 \tag{4.2}$$

$$\vec{w}_i^r = \mathsf{A}_{\mathrm{DMD}}^r \vec{w}_{i-1}^r, \quad \text{for } i = 1, \ldots, M. \tag{4.3}$$

The full-dimension form of $\vec{w}_i^r$, say $\vec{w}_i$, is computed as $\mathsf{U}_r \vec{w}_i^r$. The integer M in Eq. (4.3) is a parameter that determines how far into the future the DMD-estimated operator $\mathsf{A}_{\mathrm{DMD}}^r$ is used to predict the low-rank velocity field.

5. Reconstruction

The low-rank field $\vec{w}$ can then be used to estimate the VOF field by the optical flow map Eq. (3.2) with the displacement vector $\mathrm{d}\vec{x}$ estimated by the r-rank reconstruction,

$$\mathrm{d}\vec{X}^r = \int_t^{t+\mathrm{d}t} \vec{w}\, \mathrm{d}t. \tag{5.1}$$

Thus $\tilde{\mathcal{V}}^r(\vec{x}, \cdot)$ is the rank r approximation to $\mathcal{V}(\vec{x}, \cdot)$ given by

$$\tilde{\mathcal{V}}^r(\vec{x}, t + \mathrm{d}t) = \mathcal{V}(\vec{x} - \mathrm{d}\vec{X}^r, t). \tag{5.2}$$

A demonstration of the rank $r = 9$ reconstruction is shown in Figure 4 for $M = 2$ and $M = 20$. Visually it is apparent that the $M = 2$ estimation is more consistent with the original data whereas the $M = 20$ estimation shows several differences, most notably the reduced displacement of the right-most ligaments. The apparent reduction in the $+x$-directed translation rate is correlated with M and is a consequence of the optical flow analysis producing the interface normal vector field only. The inset in the bottom-right frame of Figure 4 demonstrates the cause: consider the cylindrical liquid region shown as translating to the right. The Horn-Schunck-estimated velocity is interface normal and therefore misses the interface-tangential component, inducing an apparent reduction in velocity.

6. Summary

A model reduction strategy has been developed to estimate the future evolution of the volume-of-fluid field present in liquid-gas multiphase flows. The multi-step approach combines image processing techniques with data-driven model reduction and has been demonstrated on a database of primary atomization of a planar liquid jet in a gas co-flow.

The method is capable of advecting the complex topology of the liquid-gas interface but cannot predict topological changes. It is therefore useful in the short-time (relative to D_ℓ/U_ℓ) prediction of atomization and sprays.

Acknowledgments

Simulation help provided by Mr. Robert Chiodi and Professor Olivier Desjardins, both at Cornell University, are gratefully acknowledged. This work was sponsored, in part, by the Office of Naval Research (ONR) as part of the Multidisciplinary University Research Initiatives (MURI) Program, under grant number N00014-16-1-2617. Computational support has been provided by the National Science Foundation XSEDE resources under grant TG-CTS090004.

REFERENCES

Desjardins, O., Blanquart, G., Balarac, G. & Pitsch, H. 2008 High order conservative finite difference scheme for variable density low Mach number turbulent flows. *Journal of Computational Physics* **227**, 7125–7159.

Dowling, A. P. & Morgans, A. S. 2005 Feedback control of combustion oscillations. *Annual Reviews of Fluid Mechanics* **37**, 151–182.

Holmes, P., Lumley, J. L. & Berkooz, G. 1996 *Turbulence, coherent structures, dynamical systems and symmetry*. Cambridge University Press.

Horn, B. K. P. & Schunck, B. G. 1981 Determining optical flow. *Artifical Intelligence* **17** (1–3), 185–203.

Hunter, H. H. 1969 A small ultrasonic atomizer for liquid fuels. *Ultrasonics* pp. 63–64.

Jansen, J.-D., Bosgra, O. H. & Van den Hof, P. M. J. 2008 Model-based control of multiphase flow in subsurface oil reservoirs. *Journal of Process Control* **18**, 846–855.

Kushari, A., Neumeier, Y., Israeli, O., Lubarsky, E. & Zinn, B. T. 2001 Internally mixed liquid injector for active control of atomization process. *Journal of Propulsion & Power* **17** (4), 878–882.

Marsh, J. F., Nunn, A. E. T. & Michelson, D. 1988 The control of electrostatic atomization using a closed-loop system. *Journal of Electrostatics* **20**, 313–318.

Neumeier, Y. & Zinn, B. T. 1996 Experimental demonstration of active control of combustion instabilities using real-time modes observation and secondary fuel injection. *Twenty-Sixth Symposium on Combustion* pp. 2811–2818.

Pratt, W. K. 2006 *Digital Image Processing*. John Wiley & Sons, Inc.

Schmid, P. J. 2010 Dynamic mode decomposition of numerical and experimental data. *Journal of Fluid Mechanics* **656**, 5–28.

Shui, L., Eijkel, J. C. T. & van den Berg, A. 2007 Multiphase flow in microfluidic systems—control and applications of droplets and interfaces. *Advances in Colloid and Interface Science* **133** (1), 35–49.